Inorg. Chem. **2007**, *46*, 5576–5584

Phenol- and Catechol-Based Ruthenium(II) Polypyridyl Complexes as Colorimetric Sensors for Fluoride Ions

D. Amilan Jose,[†] Prasenjit Kar,[†] Debasis Koley,[‡] Bishwajit Ganguly,*[,†] Walter Thiel,[‡] Hirendra N. Ghosh,*[,§] and Amitava Das*[,†]

Central Salt and Marine Chemicals Research Institute, Bhavnagar 364002, Gujarat, India, Max-Planck-Institut für Kohlenforschung, Kaiser Wilhelm-Platz 1, D-45470 Mülheim an der Ruhr, Germany, and Radiation and Photo Chemistry Division, Bhabha Atomic Research Center, Mumbai, India

Received January 30, 2007

We report two ruthenium(II) polypyridyl complexes with pendant phenol/catechol functionality that act as colorimetric sensors for fluoride ions. Experiments have revealed that hydrogen bond formation occurs with a slight excess of fluoride ion. However, in higher [F^-], deprotonation of the O–H functionality resulted. Time-dependent (TD-DFT) calculations at the B3LYP/LANL2DZ level have shown that new bands appear at longer wavelengths upon complexation with fluoride ions. These are of mixed character, MLCT ($d\pi(Ru) \rightarrow \pi^*(L_1/bpy)$), and intra- and interligand [$\pi(L_1) \rightarrow \pi^*(bpy)$ and $\pi(L_1) \rightarrow \pi^*(L_1)$] transitions. These complexes also act as sensors for fluoride ions in solvent–water mixtures.

Introduction

Selective binding of ions is an important area of research in terms of ion detection, transport, and sensing. These have a direct relevance in chemistry, biology, and environmental science.[1] Currently, there is a surge of interest in the development of tailor-made sensor molecules, able to act as chromogenic sensors for a specific analyte.[1,2] A selective sensor molecule should essentially have a receptor component specific for a selected analyte and a signaling unit capable of translating the analyte-binding induced changes into an output signal. There are numerous examples in the literature where the changes in output signals are probed by a redox potential, ^{1}H NMR chemical shifts, and/or additional spectral properties.[2−4] In the area of chromogenic sensors, fluorescence-based signaling units are generally popular for achieving high sensitivity and have low analyte detection limits.[4,5] Reports on colorimetric sensors for halides, oxyanions, and cyanide are scarce.[2,6] Current efforts have gained momentum toward the development of colorimetric sensors that are specific, and sensitive and allow visual detection of a particular analyte.[6,7] Fluoride is of particular importance

* To whom correspondence should be addressed. E-mail: ganguly@csmcri.org (B.G.), hnghosh@barc.magnum.ernet.in (H.N.G.), amitava@csmcri.org (A.D.).

[†] Central Salt and Marine Chemicals Research Institute.

[‡] Max-Planck-Institut für Kohlenforschung. E-mail: thiel@mpi-muelheim.mpg.de (W.T.).

[§] Bhabha Atomic Research Center.

(1) (a) Martinez-Manez, R.; Sancenon, F. *Chem. Rev.* **2003**, *103*, 4419. (b) Bowman-James, C. *Acc. Chem. Res.* **2005**, *38*, 671. (c) Beer, P. D.; Gale, P. A. *Angew. Chem., Int. Ed.* **2001**, *40*, 486. (d) Gale, P. A. *Coord. Chem. Rev.* **2003**, 1. (e) Suksai, C.; Tuntulani. T. *Top. Curr. Chem.* **2005**, *255*, 163. (f) Gale, P. A. *Acc. Chem. Res.* **2006**, *39*, 465.

(2) (a) Bondy, C. R.; Loeb, S. J. *Coord. Chem. Rev.* **2003**, *240*, 77. (b) Choi, K.; Hamilton, A. D. *Coord. Chem. Rev.* **2003**, *240*, 101. (c) Gale, P. A. *Coord. Chem. Rev.* **2003**, *240*, 191. (d) Suksai, C.; Tuntulani, T. *Chem. Soc. Rev.* **2003**, *32*, 192. (e) Beer, P. D. *Acc. Chem. Res.* **1998**, *31*, 71. (f) Sessler, J. L.; Davis, J. M. *Acc. Chem. Res.* **2001**, *34*, 989. (g) de Silva, A. P.; Gunaratne, H. Q. N.; Gunnlaugsson, T.; Hauxley, A. J. M.; McCoy, C. P.; Rademacher, J. T.; Rice, T. E. *Chem. Rev.* **1997**, *97*, 1515. (h) Hartley, J. H.; James, T .D.; Ward, C. J. *J. Chem. Soc., Perkin Trans.* **2000**, *1*, 3155.

(3) (a) Lee, C .H.; Lee, J. S.; Na, H. K.; Yoon, D. W.; Miyji, H.; Cho, W. S.; Sessler, J. L. *J. Org. Chem.* **2005**, *70*, 2067. (b) Ghosh, T.; Maiya, B.; Wong, M. W. *J. Phys. Chem. A* **2004**, *108*, 11249. (c) Mizukami, S.; Nagano, T.; Urano, Y.; Odani, A.; Kikuchi, K. *J. Am. Chem. Soc*. **2002**, *124*, 3902. (d) Otón, F.; Tárraga, A.; Velasco, M. D.; Espinosa, A.; Molina, P. *Chem. Commun.* **2004**, 1658. (e) Anzenbacher, P., Jr.; Try, C. A.; Miyaji, H.; Jursíková, K.; Lynch, V. M.; Marquez, M.; Sessler, J. L. *J. Am. Chem. Soc.* **2000**, *122*, 10268.

(4) (a) Lu, H.; Xu, W.; Zhang, D.; Zhu, D. *Chem. Commun.* **2005**, 4777. (b) Curiel, D.; Beer, P. D.; Cowley, A.; Sambrook M. R.; Szemes, F. *Chem. Commun.* **2004**, 1162. (c) Li, Z.-B.; Lin, J.; Zhang, H.-C.; Sabat, M.; Hyacinth, M.; Pu.; L. *J. Org. Chem.* **2004**, *69*, 6284. (d) Cho, E. J.; Moon, J. W.; Ko, S. W.; Lee, J. Y.; Kim, S. K.; Yoon, J.; Nam, K. C. *J. Am. Chem. Soc.* **2003**, *125*, 12376. (e) Xu, G. X.; Tarr, M. A. *Chem. Commun*. **2004**, 1050. (f) Curiel, D.; Cowley, A.; Beer, P. D. *Chem. Commun.* **2005**, 236.

(5) (a) Melaimi, M.; Gabbai, F. *J. Am. Chem. Soc*. **2005**, *127*, 9680. (b) Xu, S.; Chen, K.; Tian, H. *J. Mater. Chem.* **2005**, *15*, 2676. (c) Costero, A. M.; Manuel, C.; Pablo, G.; Salvador, G. *Chem. Commun.* **2006**, 761.

10.1021/ic070165+ CCC: $37.00
Published on Web 06/15/2007

due to its role in dental care and in the treatment of osteoporosis.[8] It is known that fluoride forms the strongest hydrogen bond with different donors. Urea,[9] thiourea,[9] amide,[10] pyrrole,[10] and more recently indole[11] functionalities are commonly incorporated in the design of efficient receptor units for the fluoride ion. In most cases, F^- is held to the receptor through $F^-\cdots H-N$ hydrogen-bonding interactions. The presence of excess F^- may even cause deprotonation, resulting in a classical Brønsted acid−base type reaction.[3b,12,13]

The literature contains a multitude of examples of nitrogen-based receptor molecules used for fluoride ion detection.[2−5] In stark contrast, there are only two examples where oxygen-based receptors fulfill the same role.[14a,b] ^{1}H NMR studies have shown that catechol derivatives can provide a useful binding motif for Cl^-.[14c] There are few examples in which metal polypyridyl complexes are used as the signaling unit for fluoride ion recognition. Detection has been through observing changes in redox potential, changes to the ^{1}H NMR chemical shifts, or luminescence spectral patterns.[15a,b] However, examples of the spectral change in the visible region in such Ru(II) polypyridyl complexes are rare in the literature.[15c,d]

In this paper, we report that a suitably substituted $Ru(bpy)_3^{2+}$ fragment (bpy = 2,2′-bipyridyl) with pendant phenol (**1**) or catechol (**2**) functionality can act as colorimetric sensors for fluoride ions at the ppm concentration level. Major electronic transitions for fluoride ion binding to the receptor molecules were compared with the calculated transitions using the time-dependent density functional (TD-DFT) method.

Experimental Section

Materials and Methods. Receptors **1** and **2** were synthesized by following reported procedures by the reaction of $Ru(bpy)_2Cl_2$ with 4-methyl-4′-(4-hydroxyphenyl)-2,2′-bpy (L_1) and 4-methyl-4′-(3,4-dihydroxyphenyl)-2,2′-bpy (L_2), respectively.[16] All other chemicals were of reagent grade and were used without further purification. Solvents were dried and distilled prior to use. HPLC grade acetonitrile (E. Mark, Bombay, India) was used for all spectrophotometric titrations. Solvents were degassed thoroughly with IOLAR grade dinitrogen gas before use in the preparation of standard solutions.

Microanalyses (C, H, N) were performed using a Perkin-Elmer 4100 elemental analyzer. FTIR spectra were recorded either as KBr pellets or as acetonitrile solutions in a cell fitted with a KBr window, using a Perkin-Elmer Spectra GX 2000 spectrometer. ^{1}H NMR spectra were recorded on a Bruker 200 MHz FT NMR (model: Avance-DPX 200) using CD_3CN as the solvent and tetramethylsilane (TMS) as an internal standard; ^{19}F NMR spectra were recorded with a Bruker DRX-500 spectrometer. ESI MS measurements were carried out on a Waters QTof-Micro instrument. Electronic spectra were recorded with a Shimadzu UV-3101 PC spectrophotometer; room-temperature luminescence spectra were recorded with a Perkin-Elmer LS 50B luminescence spectrofluorometer, fitted with a red-sensitive photomultiplier. Electrochemical experiments were performed on a CH-660A electrochemical instrument with a conventional three-electrode cell assembly. A saturated Ag/AgCl reference and a platinum working electrode were used for all measurements. Ferrocene was added at the end of each experiment as an internal standard and all potentials are quoted versus the ferrocene/ferrocenium (Fc/Fc^+) couple.

(6) (a) Jose, D. A.; Kumar, D. K.; Ganguly, B.; Das, A. *Org. Lett*. **2004**, *6*, 3445. (b) Jose, D. A.; Kumar, D. K.; Ganguly, B.; Das, A. *Tetrahedron Lett.* **2005**, *46*, 5343. (c) Cho, E. J.; Moon, J. W.; Ko, S. W.; Lee, J. Y.; Kim, S. K.; Yoon, J.; Nam, K. C. *J. Am. Chem. Soc.* **2003**, *125*, 12376. (d) Louise, S. E.; Gale, Philip, A.; Light, M. E.; Quesada, R. *Chem. Commun*. **2006**, 965. (e) Lin, Z-H.; Ou, S.-J.; Duan, C.-Y.; Zhang, B.-G.; Bai, Z.-P. *Chem. Commun.* **2006**, 624. (f) Jose, D. A.; Singh, A.; Das, A.; Ganguly, B. *Tetrahedron Lett*. **2007**, *48*, 3695.

(7) (a) Cho, E. J.; Ryu, B. J.; Lee, Y. J.; Nam, K. C. *Org. Lett.* **2005**, *7*, 2607. (b) Gunnalogsson, T.; Jensen, P.; Kruger, P. E. *Org. Lett.* **2005**, *7*, 5357. (c) Azenbacher, P.; Palacious, M. A.; Jursikova, K.; Marquez, M. *Org. Lett.* **2005**, *7*, 5027. (d) Gunnlaugsson, T.; Kruger, P. E.; Jensen, P.; Tierney, J.; Ali, H. D. P.; Hussey, G. M. *J. Org. Chem.* **2005**, *70*, 10875 and references therein. (e) Vázquez, M.; Fabbirizi, L.; Taglietti, A.; Pedrido, R. M.; González, N.; Bermezo, M. R. *Angew. Chem., Int. Ed.* **2004**, *43*, 1962.

(8) (a) Kirk, K. L. *Biochemistry of the Halogens and Inorganic Halides*; Plenum Press: New York, 1991; p 58. (b) Kleerekoper, M. *Endocrinol. Metab. Clin. North Am.* **1998**, *27*, 441.

(9) (a) Koulov, A. V.; Lambert, T. N.; Shukla, R.; Jain, M.; Boon, M. J.; Smith, B. D.; Li, H.; Sheppard, D. N.; Joos, J.-B.; Clare, J. P.; Davis, A. P. *Angew. Chem., Int. Ed.* **2003**, *42*, 4931. (b) Bondy, C. R.; Gale, P.; Loeb, S. J. *J. Am. Chem. Soc*. **2004**, *126*, 5030. (c) Vnzquez, M.; Fabbrizzi, L.; Taglietti, A.; Pedrido, R. M.; Gonzalez-Noya, A. M. M.; Bermejo, R. *Angew. Chem., Int. Ed.* **2004**, *43*, 1962. (d) Kwon, J. Y.; Jang, Y. J; Kim, S. K.;. Lee, K.-H.; Kim, J. S.; Yoon, J. *J. Org. Chem*. **2004**, *69*, 5155. (e) Zhang, S.; Echegoyen, L. *J. Am. Chem. Soc*. **2005**, *127*, 2006. (f) Clare, J. P.; Ayling, A. J.; Joos, J.-B.; Sission, L. A.; Magro, G.; Perez-Paynn, M. N.; Lambert, T. N.; Shukla, R.; Smith, B. D.; Davis, A. P. *J. Am. Chem. Soc*. **2005**, *127*, 10739. (g) Li, C.; Munenori, N.; Masayuki, T.; Shinkai, S. *Angew. Chem., Int. Ed.* **2005**, *44*, 6371. (h) Kim, S. K.; Singh, N. J.; Kim, S. J.; Swamy, K. M. K.; Kim, S. H.; Lee, K.-H.; Kim, K. S.; Yoon, J. *Tetrahedron* **2005**, *61*, 4545. (i) Kwon, J. Y.; Singh, N. J.; Kim, H.; Kim, S. K.; Yoon, J. *J. Am. Chem. Soc*. **2004**, *126*, 8892. (j) Kwon, J. Y.; Jang, Y. J.; Kim, S. K.; Lee, K.-H.; Kim, J. S.; Yoon, J. *J. Org. Chem.* **2004**, *69*, 5155. (k) Turner, D. R.; Paterson, M. J.; Steed, J. W. *J. Org. Chem.* **2006**, *71*, 1598.

(10) (a) Nishiyabu, R.; Anzenbacher, P., Jr. *Org. Lett.* **2006**, *8*, 359. (b) Nielsen, K. A.; Cho, W.-S.; Lyskawa, J.; Levillain, E.; Lynch, V. M.; Sessler, J. L.; Jeppesen, J. O. *J. Am. Chem. Soc*. **2006**, 128, 2444 and reference therein. (c) Sessler, J. L.; Katayev, E.; Pantos, G. D.; Scherbakov, P.; Reshetova, M. D.; Khrustalev, V. N.; Lynch, V. M.; Ustynyuk, Y. A. *J. Am. Chem. Soc*. **2005**, *127*, 11442. (d) Sessler, J. L.; Davis, J. M. *Acc. Chem. Res.* **2001**, *34*, 989. (e) Sessler, J. L.; Camiolo, S.; Gale, P. A. *Coord. Chem. Rev*. **2003**, *240*, 17. (f) Gale, P. A. *Chem. Commun*. **2005**, 3761. (g) Evgeny, A. K; DanPantos, G.; Reshetova, M. D.; Khrustalev, V. N.; Lynch, V. M; Ustynyuk, Y. A.; Sessler, J. L. *Angew. Chem., Int. Ed.* **2005**, *44*, 7386. (h) Kang, S. O.; Powell, D.; Day, V. W.; Bowman-James, K. *Angew. Chem., Int. Ed.* **2006**, *45*, 1921.

(11) (a) Curiel, D.; Cowley, A.; Beer, P. D. *Chem. Commun*. **2005**, 236. (b) Chang, K-J.; Dohyun, Moon, D.; Lah, M. S.; Jeong, K. S. *Angew. Chem., Int. Ed.* **2005**, *44*, 7926.

(12) (a) Boiocchi, M.; Del Boca, L.; Gomez, D. E.; Fabbrizzi, L.; Licchelli, M.; Monazani, E. *J. Am. Chem. Soc*. **2004**, *126*, 16507. (b) Gomez, D. E.; Fabbrizzi, L.; Licchelli, M.; Monazani, E. *Org. Biomol. Chem*. **2005**, *3*, 1495.

(13) (a) Peng, X.; Wu, Y.; Fan, J.; Tian, M.; Han, K. *J. Org. Chem.* **2005**, *70*, *10524*. (b) Gomez, D. E.; Fabbrizzi, L.; Liccheli, M. *J. Org. Chem.* **2005**, *70*, 5717. (c) Gronert, S. *J. Am. Chem. Soc.* **1993**, *115*, 10258.

(14) (a) Miyaji, H.; Sato, W.; Sessler, J. L *Angew. Chem., Int. Ed.* **2000**, *39*, 1777. (b) Lee, K. H.; Lee, H. Y.; Lee, D. H.; Hong, J. I. *Tetrahedron Lett*. **2001**, *42*, 5447. (c) Smith, D. K. *Org. Biomol. Chem*. **2003**, *1*, 3874.

(15) (a) Beer, P. D.; Hayes, E. J. *Coord. Chem. Rev.* **2003**, *240*, 167 and references therein. (b) Anzenbacher, P.; Tyson, D. S.; Jursikova, K.; Castellano, F. N. *J. Am. Chem. Soc*. **2002**, *124*, 6232. (c) Mizuno, T.; Wei, W.-H.; Eller, L. R.; Sessler, J. L. *J. Am. Chem. Soc*. **2002**, *124*, 1134. (d) Lin, Z. H.; Ou, S. J; Duan, C. Y.; Zhang, B. G.; Bai, Z. P. *Chem. Commun.* **2006**, 624.

(16) (a) Shukla, A. D.; Whittle, B.; Bajaj, H. C.; Das, A.; Ward, M. D. *Inorg. Chim. Acta* **1999**, *285*, 89. (b) Amoroso, A. J.; Das, A.; McCleverety, J. A.; Ward, M. D.; Barigelletti, F.; Flamigni, L. *Inorg. Chim. Acta* **1994**, *226*, 171. (c) Ramakrishna, G.; Jose, D. A; Kumar, K. K.; Das, A.; Palit, D. K; Ghosh, H. N. *J. Phys. Chem. B* **2005**, *109*, 15445.

Spectrophotometric Titration. Several 1.0×10^{-4} M solutions of the complexes **1** and **2** in acetonitrile were prepared and stored in dark. These solutions were used for all spectroscopic studies after appropriate dilution. The 1.0×10^{-3} M solutions of tetrabutylammonium salts of the respective anions were prepared in dried and distilled acetonitrile and were stored under an inert atmosphere. All titration experiments were performed using 2.0×10^{-5} M solutions of complex **1** or 1.25×10^{-5} M solutions of **2** in acetonitrile and various concentrations of anions (2.0×10^{-6}−1.0×10^{-4} M) in the same solvent. Affinity constants were evaluated after calculating the concentrations of the respective species, free **1** and **2**, F^-, and associated complexes, e.g., **1**·F^- (1:1 complex of receptor **1** and F^-**)** and **2**·F^- (1:1 complex of receptor **2** and F^-). The effect of the ionic strength on the affinity constant was also examined by repeating the studies at various (0−0.1 M $[nBu_4N]ClO_4$) supporting electrolyte concentrations. Affinity constants were evaluated from the collected absorbance data of the titration curve using 540 nm as the probe wavelength, and the equation $K = [LA^-]/\{[L]_{free}[A^-]_{free}\}$was used for all calculations (Supporting Information).

Luminescence Titration. The standard solutions mentioned above were used for spectrophotometric titrations and luminescence titration studies. For all measurements, $\lambda_{ext} = 458$ nm with an excitation and emission slit width of 7 nm. All titration experiments were performed using 5.0×10^{-5} M solutions of complex **1** and **2** in acetonitrile (degassed before measurement with IOLAR grade dinitrogen gas saturated with acetonitrile vapor) and solutions of various anions (2.0×10^{-6}−5.0×10^{-3} M) in acetonitrile.

Computational Details. All the calculations were performed using the Gaussian 03 program suite.[17] The DFT calculations employed the B3LYP function and the standard double-ζ LANL2DZ basis set along with the corresponding pseudopotential for ruthenium.[18,19] The LANL2DZ basis set for the electronegative fluorine atom was augmented with an extra d-function.[20] Both the ligands and the complexes were fully optimized in acetonitrile ($\epsilon = 36.64$) using the "polarizable continuum model" (PCM)[21] as implemented in Gaussian 03.

The TD-DFT singlet excitation energies of the complexes in acetonitrile were evaluated by a recent nonequilibrium implementation of the conductor-like polarizable continuum model (CPCM).[22] In the calculation of the optical spectra, the 140 lowest spin-allowed singlet−singlet transitions, up to an energy of ∼5.6 eV, were taken into account. Transition energies and oscillator strengths were interpolated by a Gaussian convolution with a width of 0.2 eV.

Results and Discussion

Electronic Spectral Studies. Ru(II) polypyridyl receptor molecules, **1** and **2**, were synthesized by following reported procedures and were characterized using standard spectroscopic and analytical techniques.[23] The electronic spectra recorded for both these complexes in acetonitrile are shown in Figure 1. The observed transition bands at 280, 340, and 455 nm for ruthenium(II) polypyridyl complexes were assigned to be predominantly intraligand bpy/L_1/L_2-based $\pi \rightarrow \pi^*$, interligand bpy/L_1/L_2-based $\pi \rightarrow \pi^*$, and $d\pi_{Ru} \rightarrow \pi^*_{bpy}/\pi^*_{L1/L2}$ transitions on the basis of TD-DFT calculations. To these receptors, a solution of $[nBu_4N]F$ in CH_3CN was added. We observed a distinct color change from red to dark violet for **1** and brown for **2** (Figure 2). The colors persisted when water (≤20%; v/v) was added. The UV−vis spectra recorded for these solutions showed the disappearance of an absorption maximum at 348 nm and the appearance of a new absorption band at ca. 550 nm (Figure 1).

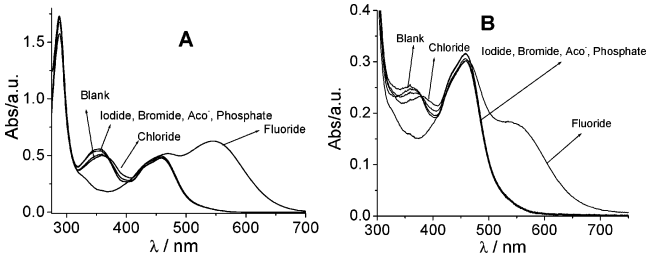

Figure 1. Change in the UV−vis spectra for (A) receptor **1** (2.0×10^{-5} M) and (B) **2** (1.25×10^{-5} M) at RT in acetonitrile in the absence and presence of different anions (excess).

When a large excess of F^- was added, an intense absorption band at 550 nm appeared, more intense for **1** than **2**, and the corresponding molar absorptivity values determined were 2.49×10^4 and 1.02×10^4 M^{-1} cm^{-1}, respectively. A color change was not observed for CN^-, Br^-, Cl^-, I^-, or oxyanions (e.g., $H_2PO_4^-$, $CH_3CO_2^-$, $PhCO_2^-$,

(17) Frisch, M. J.; et. al. *Gaussian 03*, revision B.04; Gaussian, Inc.: Pittsburgh, PA, 2003.

(18) (a) Becke, A. D. *Phys. Rev. A* **1988**, *38*, 3098. (b) Becke, A. D. *J. Chem. Phys.* **1993**, *98*, 5648. (c) Lee, C.; Yang, W.; Parr, R. G. *Phys. Rev. B* **1988**, *37*, 785.

(19) (a) Dunning, T. H., Jr.; Hay, P. J. *Modern Theoretical Chemistry*; Plenum: New York, 1976; Vol. 3. (b) Hay, P. J.; Wadt, W. R. *J. Chem. Phys.* **1985**, *82*, 270. (c) Hay, P. J.; Wadt, W. R. *J. Chem. Phys.* **1985**, *82*, 299. (c) Hay, P. J.; Wadt, W. R. *J. Chem. Phys.* **1985**, *82*, 284.

(20) Dunning, T. H., Jr.; Hay, P. J. *Methods of Electronic Structure Theory*; Schaefer, H. F., III, Ed.; Plenum Press: New York, 1977; Vol. 2.

(21) (a) Miertuš, S.; Scrocco, E.; Tomasi, J. *Chem. Phys.* **1981**, *55*, 117. (b) Cossi, M.; Barone, V.; Cammi, R.; Tomasi, J. *Chem. Phys. Lett.* **1996**, *255*, 327.

(22) (a) Klamt, A.; Schüürmann, G. *J. Chem. Soc., Perkin Trans. 2* **1993**, 799. (b) Klamt, A.; Jonas, V. *J. Chem. Phys.* **1996**, *105*, 9972.

(23) Analytical data for L_1: Anal. Found: C, 79.6; H, 5.5; N, 9.6. Calcd: C, 79.1; H, 5.6; N 9.7. ES-MS: *m/z* 288 (M^+, 100%). ^{1}H NMR (DMSO-d_6, ppm): δ 9.77 (−OH proton), 8.61 (1H, d, $J = 5.6$ Hz, H_6), 8.57 (1H, d, $J = 5.6$ Hz; bpy′ $H_{6'}$), 8.47 (1H, s; bpy′ H_3), 8.25 (1H, s; bpy′ $H_{3'}$), 7.49−7.57 (4H, m, $H_{5'}$, phenyl H_2 and H_6, and ethenyl), 7.30 (1H, d, $J = 5.6$ Hz; bpy′ H_5), 7.14 (1H, d, $J = 16.6$ Hz, ethenyl), 6.81 (2H, d, $J = 8.3$ Hz; phenyl), 2.42 (3H, s, $-CH_3$). Analytical data for L_2: Anal. Found: C, 74.6; H, 5.8; N, 9.0. Calcd: C, 74.9; H, 5.3; N 9.2. ES-MS: *m/z* 304 (M^+, 100%), 289 ($M^+ - CH_3$, 50%). ^{1}H NMR (CD_3OD, ppm): δ 8.55 (2H, d, $J = 5.8$ Hz, bpy′ H_6, $H_{6'}$), 8.25 (1H, s; bpy′ H_3), 7.68 (1H, d, $J = 5.1$ Hz; bpy′ H_5), 7.58 (1H, d, $J = 16.3$ Hz; −ethenyl), 7.43 (1H, d, $J = 5.2$ Hz; bpy′ $H_{5'}$), 7.13 (1H, d, $J = 8.0$ Hz, phenyl H_2), 7.00−7.07 (2H, m, phenyl H_6, and ethenyl), 6.79 (1H, d, $J = 8.1$ Hz; phenyl H_5), 2.56 (3H, s; $-CH_3$). Analytical data for complex **1**: Anal. Found: C, 47.0; H, 3.2; N, 8.4. Calcd: C, 47.2; H, 3.3; N, 8.5. ES-MS: *m/z* 847 ($M - PF_6$)$^+$ (20%), 702 ($M - 2PF_6$)$^+$ (10%). ^{1}H NMR (CD3CN, ppm): δ 8.5 (6H, d, 6.6 Hz, $2H_6$(bpy), $2H_{6'}$(bpy) H_6 and $H_{6'}$ L1), 8.06 (4H, t, $J = 7.8$ Hz, $2H_4$ (bpy), $2H_{4'}$ (bpy)), 8.02, (1H, s, $H_3(L_1)$), 7.82 (1H, d, $J = 5.4$ Hz, $H_{3'}$ (L_1)), 7.74−7.52 (5H, m, $2H_5$ (bpy), $2H_{5'}$ (bpy), ethenyl)), 7.44−7.75 (6H, m, $2H_3$ (bpy), $2H_{3'}$ (bpy), $2H_{3,5}$ (phenyl)), 7.35 (1H, d, $J = 6.6$ Hz, H_5 (L_1)), 7.24 (1H, d, $J = 6.6$ Hz, $H_{5'}$ (L_1)), 7.08 (1H, d, $J = 16.6$ Hz, ethenyl), 6. 88 (2H, d, $J = 8.6$ Hz, $H_{2,6}$ (phenyl)), 2.56 (3H, s; −CH3). IR (KBr pellet, cm^{-1}): 3449 (−OH), 1603 (C═C, C═N), 846 (PF6). Analytical data for complex **2**: Anal. Found: C, 46.7; H, 3.2; N, 8.1. Calcd: C, 46.5; H, 3.2; N, 8.3. ES-MS: *m/z* 863 ($M - PF6$)$^+$ (15%), 717 ($M - 2PF6$)$^+$ (5%). ^{1}H NMR (CD3CN, ppm): δ 8.5 (6H, d, 6.6 Hz, $2H_6$ (bpy), $2H_{6'}$ (bpy) H_6 and $H_{6'}$ L1), 8.07 (4H, t, $J = 7.6$ Hz, $2H_4$ (bpy), $2H_{4'}$ (bpy)), 8.01 (1H, s, H_3 (L_1)), 7.82 (1H, d, $J = 5.8$ Hz, $H_{3'}$ (L_1)), 7.76−7.56 (5H, m, $2H_5$ (bpy), $2H_{5'}$ (bpy), ethenyl), 7.43−7.35 (6H, m, $2H_3$ (bpy), $2H_{3'}$ (bpy), $2H_{5,5'}$ (L_1)), 7.23 (1H, d, $J = 8.2$ Hz, H_5 (phenyl)), 7.03 (1H, d, $J = 8.2$ Hz, H_6 (phenyl)), 7.13 (1H, d, $J = 16.6$ Hz, ethenyl), 6.86 (1H, d, $J = 8.2$ Hz, H_3 (phenyl)), 2.56 (3H, s; −CH3). IR (KBr pellet, cm^{-1}): 3449 (−OH), 1603 (C═C, C═N), 844 (PF6).

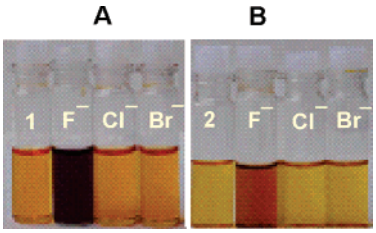

Figure 2. Color changes inducted by the addition of anions (tetrabutylammonium salts). From left to right: (A) receptor **1**, **1** + F^-, **1** + Cl^-, and **1** + Br^-; (B) color changes for receptor **2**, **2** + F^-, **2** + Cl^-, and **2** + Br^-.

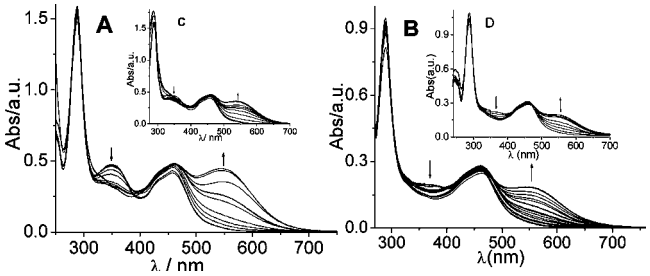

Figure 3. Change in electronic spectra for acetonitrile solutions of (A) receptor **1** (2.0×10^{-5} M) at RT for different [F^-] ($(0.50-10) \times 10^{-5}$ M) and (B) receptor **2** (1.25×10^{-5} M) at RT for varying [F^-] ($(0.50-20) \times 10^{-5}$ M). Inset: Figures show similar spectral changes with 5.0×10^{-6}–2.0×10^{-4} M [nBu_4N]OH for (C) **1** and (D) **2**.

NO_2^-, HSO_4^-, etc.) (Figure 1). Addition of F^- to a solution of **1** or **2** (5.0×10^{-5} M in degassed CH_3CN) decreased the emission intensity ($\lambda_{max} = 605$ nm for **1** and $\lambda_{max} = 600$ nm for **2**; $\lambda_{ex} = 458$ nm) by a factor of 3−3.5. A detectable change in color and a decrease in the emission intensity on addition of F^- suggests that there is strong hydrogen bonding between F^- and the phenolic functionality of **1** and **2**. However, supporting evidence for this from similar systems are scarce and a quantitative study on binding affinity is not available from the literature to date.[14a]

Furthermore, the control experiments with $Ru(bpy)_3^{2+}$ and F^- did not show any spectral change in the absorption and emission spectrum, confirming that the phenolic functionalities of **1** and **2** are involved in hydrogen bonding with the fluoride ion. Systematic changes in the electronic spectra on addition of standard F^- solutions ($(0.5-3.75) \times 10^{-5}$ M in CH_3CN) to the respective solution (in CH_3CN) of **1** (2.0×10^{-5} M) or **2** (1.25×10^{-5} M) are shown in Figure 3. For **1**, a hypochromic shift at ca. 353 nm with an isosbestic point at 384 nm and a hyperchromic shift from 456 nm to 480−625 nm with an increase in absorbance until the addition of ca. 1.2 equiv of F^- was observed (Figure S1).

A binding isotherm for this titration experiment revealed that **1**·F^- formed when 2.0×10^{-5} M (in CH_3CN) **1** was titrated with 0.5×10^{-5}−3.5×10^{-5} M (in CH_3CN) F^- (Figure S3); the evaluated affinity constant value ($K_1(F^-)$) was 4.93×10^5 M^{-1}. A more significant change in absorbance at 550 nm was observed upon further addition ($3.5-10 \times 10^{-5}$ M) of F^- (Figure S1), and a new isosbestic point was observed at ca. 474 nm. The corresponding equilibrium constant was 6.56×10^3 M^{-1}. A similar change in the spectral pattern was observed for **2** with the isosbestic point at 394 nm, and the increase in absorbance within the spectral range 480−625 nm was less prominent. The binding isotherm

Table 1. Equilibrium Constants for **1** and **2** toward Cl^- and F^- Binding[a]

	affinity/dissociatn const[b,c] ($M^{-1}/10^3$)			
reacn	$K_n(F^-)$	$K_n^d(F^-)$	$K_n(Cl^-)$	$K_n^d(OH^-)$
1 + X^-	490 ± 20	6.6 ± 0.2	0.15 ± 0.02	60 ± 3
2 + X^-	520 ± 20	12 ± 1	0.17 ± 0.01	173 ± 10

[a] Tertiary butyl salts of respective anions were used. [b] *K* values reported are the average of 10 independent data evaluated from UV−vis titration data for the respective receptor and anion. [c] *n* is 1 for complex **1** and 2 for complex **2**; confidence limits for the respective *K* values are given.

for **2** also showed the formation of **2**·F^-, with an equilibrium constant of 5.16×10^5 M^{-1} (Figures S2 and S4). The increase in absorbance at 540 nm was more intense upon addition of F^- ($4.75-20.0) \times 10^{-5}$ M in CH_3CN). However, no well-resolved spectral band was observed, as had been evident in case of receptor **1** (Figures S2 and S4). A new isosbestic point for this set of spectrophotometric titrations appeared at 486 nm. The equilibrium constant for this titration was found to be 1.17×10^3 M^{-1}. Two equilibrium constants detected for each of **1** and **2** differ by a factor of at least 50, which leads to two well-defined inflection points (Table 1).

The titration profile for the second inflection point revealed that the [receptor]:[F^-] ratios for **1** and **2** were 0.3 and 0.25, respectively. Fabbrizi et al. and later researchers have shown that suitably substituted H-bond donor receptor functionality undergo deprotonation in the presence of excess F^-, leading to classical Brønsted acid−base chemistry and is not commonly believed as a supramolecular interaction.[12,24] It has been argued that the higher stability of a polynuclear aggregate, such as HF_2^-, further facilitates the deprotonation of the receptor unit.[3b,13,24] To examine such a possibility in **1** and **2**, spectrophotometric titrations of **1** (2.0×10^{-5} M) and **2** (1.25×10^{-5} M) were carried out in a standard solution (5.0×10^{-6}−2.0×10^{-4} M; 0.5−8 equiv) of [nBu_4N]OH (Figure 3). For **1** and **2**, the equilibrium for the H-bond formation ($HO^-\cdots H-O$), could not be distinguished; however, the proton dissociation constants could be obtained ($K_1^d = 6.0 \times 10^4$ M^{-1} and $K_2^d = 1.73 \times 10^5$ M^{-1}). These dissociation constants suggest that the catechol hydroxyl group in **2** is more acidic than in **1** (Scheme 1). Molar absorptivity values obtained for $\mathbf{1}_{-H}^-$ at λ_{469} and λ_{535} are 1.77×10^4 and 1.86×10^4 M^{-1} cm^{-1}, respectively. For $\mathbf{2}_{-H}^-$ these values are 2.03×10^4 M^{-1} cm^{-1} (λ_{460}) and 1.50×10^4 M^{-1} cm^{-1} (λ_{535}), respectively. The deprotonated spectral patterns for **1** and **2** (deprotonation achieved using [(nBu_4N]-OH) have close resemblance to the spectra of these receptors in excess (>4 equiv) F^- (insert in Figure 3). These observations suggest that, in a large excess of F^-, the Brønsted acid−base reaction prevails, whereas, in a slight excess (~1.5 equiv), hydrogen-bonding [$F^-\cdots H-O$] interac-

(24) (a) Amendola, V.; Esteban-goä mez, D.; Fabbrizzi, L.; Licchelli, M. *Acc. Chem. Res.* **2006**, *39*, 343. (b) Boiocchi, M.; Boca, L. D.; Gomez, D. E.; Fabbrizzi, L; Licchelli, M.; Monzani, E. *Chem.—Eur. J.* **2005**, *11*, 3097. (c) Amendola, V.; Boiocchi, M; Fabbrizzi, L; Palchetti, *A. Chem.—Eur. J.* **2005**, 11, 5648. (d) Peng, X.; Wu, Y.; Fan, J.; Tian, M.; Han, K. *J. Org. Chem.* **2005**, *70*, 10524. (e) Gunnlaugasson, T.; Kruger, P. E.; Jensen, P.; Tierney, J; Ali, H. D. P.; Hussey, G. M. *J. Org. Chem.* **2005**, *70*, 10875. (f) Amendola, V.; Boiocchi, D.; Colasson, B.; Fabbrizzi, L. *Inorg. Chem.* **2006**, *45*, 6138.

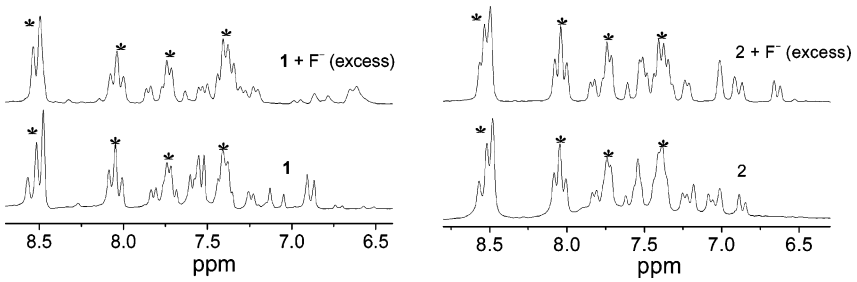

Figure 4. Partial ^{1}H NMR (200 MHz) spectra of receptors in CD_3CN at RT with 5.0 equiv of $[nBu_4N]F$ (A) for receptor **1** and (B) for receptor **2**. Asterisks indicate signals due to protons belonging to the bpy group.

Scheme 1

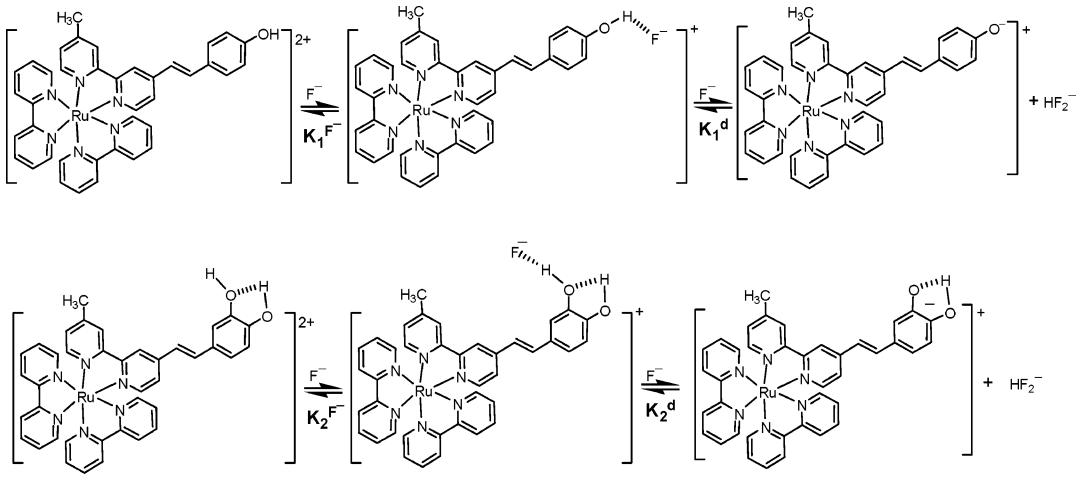

tions are operative. Observation of the second deprotonation in the case of **2** did not occur, possibly due to the stability of the intramolecular H-bonding (Scheme 1).

The two equilibrium processes involved in the titration with F^- support Fabbrizzi's proposition and are shown in Scheme 1. In the scheme, the second equilibrium constants obtained from the spectrophotometric titrations for **1** and **2** with F^- are assigned as K_1^d and K_2^d (proton dissociation) and the formation of HF_2^- is illustrated. No change in color or spectral pattern was observed for other anions ($X^- = Br^-$, I^-, CH_3COO^-, $H_2PO_4^-$, NO_2^-, HSO_4^-, CN^-, and BF_4^-). A minor change in spectral pattern was observed only for Cl^- (Figure 1 and Table 1).

^{1}H NMR Studies. ^{1}H NMR spectra for **1** and **2** were recorded (CD_3CN) in the absence and presence of varying $[F^-]$. An upfield shift was observed for the protons of L_1 and L_2 in the respective complexes of **1** and **2**. However, shifts for the bpy protons were less appreciable (Figure 4).[25] The upfield shifts signify the increase in electron density in L_1 or L_2 through bonding effects in **1**$\cdots$**F**$^-$/**1**$_{-H}^-$ or **2**$\cdots$**F**$^-$/**2**$_{-H}^-$. This supports the formation of an intramolecular hydrogen bond as proposed in Scheme 1. It may be mentioned here that in the absence of any change to the optical spectral pattern the possibility of a weaker $X^-\cdots H-O$ interaction between **1** and **2** with X^- ($X^- = Br^-$, I^-, CH_3COO^-, $H_2PO_4^-$, CN^-, NO_2^-, and HSO_4^-) cannot be ruled out. This was further resolved in ^{1}H NMR studies.[26] Equilibrium constants for the binding of F^- to **1** and **2** and their proton dissociation values were also evaluated using ^{1}H NMR titration experiments in CD_3CN. The association constants ($K_n(F^-)$, where n = 1 and 2 for complexes 1 and 2, respectively) obtained via the latter for **1** and **2** with F^- are 2.25×10^5 and 2.32×10^5 M^{-1}, respectively. These values closely match the values calculated using the UV−vis absorption titration method. The basic equation used for the titrations that defines the relationship among chemical shifts (δ), concentrations of host H, guest G, and complex C, and the binding constant K_b is shown in eq 1.[27] Upon addition of fluoride ions, the downfield shift in the values at δ 6.91 ppm for **1** and δ 6.66 ppm for **2** have been considered to calculate the association constant.

$$\delta_{OBS} = (\delta_C - \delta_H)(\{(1 + [G]/[H] + 1/K_b[H])/2\} - \{(1 + [G]/[H] + 1/K_b[H])^{2/4} - [G]/[H]\}^{1/2}) + \delta_H \quad (1)$$

^{19}F NMR spectra recorded for (TBA)F/**1** and (TBA)F/**2** (1:1.2 mol equiv) clearly showed the formation of hydrogen-

(25) **1**$\cdots$**F**$^-$: ^{1}H NMR (CD3CN, ppm) δ 8.51 (6H, d, 6.7 Hz, $2H_6$ (bpy), $2H_{6'}$ (bpy) H_6 and $H_{6'}$ L1), 8.04 (4H, t, J = 7.6 Hz, $2H_4$ (bpy), $2H_{4'}$ (bpy), 7.59 (1H, d, J = 16.2 Hz, ethenyl), 7.53 (1H, s, $H_3(L_1)$), 7.50 (1H, s, $H_{3'}$ (L_1)), 7.74 (4H, d, J = 7.6 Hz, $2H_3$, $2H_{3'}$ (bpy)), 7.41−7.34 (6H, m, $2H_5$ (bpy), $2H_{5'}$ (bpy), $2H_{3,5}$ (phenyl)), 7.23 (1H, d, J = 6.7 Hz, H_5 (L_1)), 7.24 (1H, d, J = 6.6 Hz, $H_{5'}$ (L_1), 6.83 (1H, d, J = 16.2 Hz, ethenyl), 6. 58 (2H, d, J = 7.8 Hz, $H_{2,6}$ (phenyl)), 2.54 (3H, s; $-CH_3$); ES-MS m/z 993 (M^+) (60%), 1010.9 ($M^+ + F^-$) (10%), 865 ($M^+ - PF_6 + F^-$) (40%), 702 ($M^+ - 2PF_6$) (12%), 721 ($M^+ - 2PF_6 + F^-$) (9%). **2**$\cdots$**F**$^-$: ^{1}H NMR (CD_3CN, ppm) δ 8.51 (6H, d, 6.8 Hz, $2H_6$ (bpy), $2H_{6'}$ (bpy), H_6 and $H_{6'}$ (L_2)), 8.06 (4H, t, J = 7.8 Hz, $2H_4$ (bpy), $2H_{4'}$ (bpy)), 8.00 (1H, s, $H_3(L_2)$), 7.84 (1H, d, J = 5.2 Hz, $H_{3'}$ (L_2)), 7.77−7.48 (5H, m, $2H_5$ (bpy), $2H_{5'}$ (bpy), ethenyl), 7.44−7.34 (6H, m, $2H_3$ (bpy), $2H_{3'}$ (bpy), H_5, $H_{5'}$ (L_2)), 7.24 (1H, d, J = 8.2 Hz, H_5 (phenyl)); 6.96 (1H, d, J = 16.4 Hz, ethenyl), 6.87 (1H, d, J = 8.2 Hz, H_6 (phenyl)), 6.6 (1H, d, J = 8.0 Hz, H_3 (phenyl)), 2.56 (3H, s, $-CH_3$); ES-MS 1008 (M^+) (50%), 863 ($M^+ - PF_6$) (12%), 717 ($M^+ - 2PF_6$) (25%), 736 ($M^+ - 2PF_6 + F^-$) (7%).

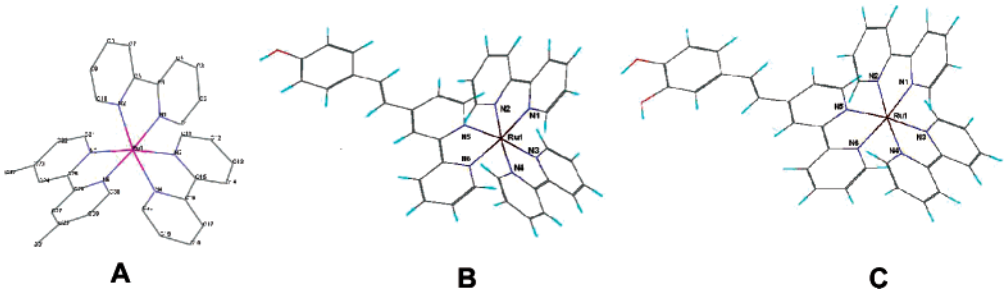

Figure 5. (A) Crystal structure of $[RuL_3]^{2+}$ (L = 4,4′-dimethyl-2,2′-bpy) [Hesek, D.; Inoue, Y.; Everitt, S. R. L.; Ishida, H.; Kunieda, M.; Drew, M. G. B. *Chem. Commun.* **1999**, 403]. (B, C) Optimized structure of the receptors **1** and **2**, respectively.

Table 2. $E_{1/2}$ Values Recorded for **1** and **2** in the Absence and Presence of Excess F^- or OH^- [a]

	$E_{1/2}$/V (vs Fc/Fc^+)				
complex	$Ru^{II/III}$	oxolene	L_1/L_2	bpy	bpy
1	0.93 (100)		−1.725 (85)	−1.925 (95)	−2.21 (110)
$\mathbf{1}_{-H}^-$ (F^-, 1.2 equiv)	0.92 (90)		−1.77 (90)	−1.96 (90)	−2.19[b]
$\mathbf{1}_{-H}^-$ (OH^-, 1.2 equiv)	0.92 (95)		−1.78 (90)	−1.96 (100)	−2.22[b]
2	0.92 (95)	0.68[c]	−1.76 (85)	−1.97 (85)	−2.23 (120)
$\mathbf{2}_{-H}^-$ (F^-, 1.2 equiv)	0.93 (100)	∼0.6[c,d]	−1.805 (95)	−2.015 (110)	−2.24[b]
$\mathbf{2}_{-H}^-$ (OH^-, 1.2 equiv)	0.92 (95)	∼0.6[c,d]	−1.81 (100)	−2.00 (110)	−2.24[b]

[a] $E_{1/2}$ values were recorded as CH_3CN solutions. For the reported potential values, a scan rate of 100 mV s^{-1} was used. Uncertainty in the measurement of the $E_{1/2}$ values is ±0.01 mV. Waves that were clearly reversible have the peak−peak separation (mV) in parentheses. [b] Quasi reversible redox process. [c] Irreversible redox process (swv data). [d] Redox wave (swv data) was very broad, possibly due to the presence of more than one overlapping redox wave.

bonded species with the appearance of ^{19}F signals at ca. −122 and 112 ppm for (TBA)F. For (TBA)F/**1** and (TBA)F/**2** (1:2 mol equiv) solutions, ^{19}F signals appeared for the formation of $\mathbf{1}\cdots\mathbf{F}^-$ and $\mathbf{2}\cdots\mathbf{F}^-$ at −122 and −151 ppm for the HF_2^- species (Figure S10).[10h]

FTIR Studies. FTIR spectra for **1** and **2** were recorded in acetonitrile solutions in the absence and presence of fluoride ions. The expected bands for the −OH functionality and C═C/C═N and PF_6^- units were observed in the absence of fluoride. When spectra were recorded in the presence of 1 equiv or an excess of F^-, the stretching frequency of the −OH group shifted to a lower energy. For **1**, it was found to shift from 3485 to 3478 cm^{-1}. A similar shift was observed for **2** from 3482 to 3478 cm^{-1}. Shifts for the −O−H functionalities on H-bonding are also reported.[28] Mass spectral data also support the formation of such adducts ($\mathbf{1}.\mathbf{F}^-$ and $\mathbf{2}.\mathbf{F}^-$).[25]

Electrochemical Studies. Cyclic voltammograms recorded for **1** and **2** showed the expected metal-based Ru(II/III) redox couple at ca. 0.92 V. Ligand-based redox potentials were observed as follows: L_1- or L_2-based $L_1/L_1^{\bullet-}$ or $L_2/L_2^{\bullet-}$ redox couple at ca. −1.65 V and two bpy-based bpy/bpy$^{\bullet-}$ redox couples at ca. −2.0 and ca. −2.3 V (Table 2). Cyclic voltammograms and in certain cases square wave voltammograms (swv) were recorded in the presence of varying [F^-], and there was no noticeable change in the $E_{1/2}$ values for the Ru(II/III) couple. However, a general cathodic shift of 35−45 mV was observed for one of the two coordinated bpy molecules and for the L_1- or L_2-based redox processes. The $E_{1/2}$ values for the same redox couple of the other bpy ligand remain unaffected (Table 2).

This shift may be ascribed to the increased electron density on L_1/L_2 due to deprotonation of the −OH functionality in **1** or **2**. This interpretation also agreed well with the upfield shift observed for the $H_{CH=CH}$ protons and the other phenyl ring protons in the ^1H NMR spectra recorded for $\mathbf{1}_{-H}^-$ or $\mathbf{2}_{-H}^-$. The irreversible nature of the catechol-based redox couple for **2** at +0.68 V makes comment on the shift associated with this redox process difficult. There are very few examples in the literature where Ru(II) polypyridyl based complexes have been used as anion sensors.[15c,d] Similar growth in the absorbance on anion binding induced changes in the electronic spectra have been reported. To understand the observed shift in the absorption spectral pattern on F^- ion binding, we have performed time-dependent density functional (TD-DFT) calculations.

Computational Studies. The geometries of **1** and **2** have been optimized at the B3LYP/LANL2DZ level. The structural parameters calculated for **1** and **2** were found to be in good agreement with those for a closely related complex, for which X-ray structural data had been reported (Figure 5 and Table 3).

The optimized structures possess pseudooctahedral coordination at the RuN_6 core, with N−Ru−N angles close to 80°. The L_1 and L_2 units attached to the $Ru(bpy)_2$ core were planar in both **1** and **2** (Figure 5). In the case of **2**, the hydroxy groups formed an intramolecular hydrogen bond leaving one of the OH hydrogen atoms (*meta* to the vinyl linkage) to interact with the fluoride ion (Figure 5). One should note that the published DFT (TD-DFT) studies on

(26) On addition of different halide ions (Cl^-, Br^-, I^-) to receptor **1**, the signal for H_{OH} shifts from 8.57 to 9.44 (br), 8.91 (s), and 8.77 (m) respectively for Cl^-, Br^-, and I^-. An upfield shift in C−H protons of the phenolic and ethylenic H atoms was observed, though the extent of shift was much smaller compared to that observed for F^-. The extent of shift follows the order F^-, Cl^-, and Br^-.

(27) (a) Fielding, L. *Tetrahedron* **2000**, *56*, 6151. (b) Heath, R. E.; Dykes, G. M.; Fish, H.; Smith, D. K. *Chem.—Eur. J.* **2003**, *9*, 850.

(28) (a) Gerhards, M.; Unterberg, C.; Kleinermanns, K. *Phys. Chem. Chem. Phys.* **2000**, *2*, 5538. (b) Fujii, A.; Ebata, T.; Mikami, N. *J. Phys. Chem. A* **2002**, *106*, 8554.

Table 3. Selected Geometrical Parameters for **1** and **2** Obtained from DFT Studies (Bond Lengths in Å; Angles in deg)

	bond lengths				bond angles		
param	$(RuL_3)^{2+}$ [a]	calcd for **1**	calcd for **2**	compd	param	$(RuL_3)^{2+}$ [a]	calcd
Ru−N1	2.077(5)	2.096	2.094	**1**	N1RuN2	79.08	78.518
Ru−N2	2.059(5)	2.095	2.095		N3RuN4	78.28	78.570
Ru−N6	2.062(5)	2.095	2.095		N5RuN6	78.1	78.409
Ru−N4	2.076(5)	2.097	2.097	**2**	N1RuN2	79.09	78.560
Ru−N5	2.055(6)	2.095	2.095		N3RuN4	78.28	78.505
Ru−N6	2.069(5)	2.097	2.097		N5RuN6	78.1	78.697

[a] Selected X-ray data for $[RuL_3]^{2+}$ (L is 4,4′-dimethyl-2,2′-bpy). Values are quoted from the following: Hesek, D.; Inoue, Y.; Everitt, S.R.L.; Ishida, H.; Kunieda, M.; Drew, M. G. B. *Chem. Commun*. **1999**, 403.

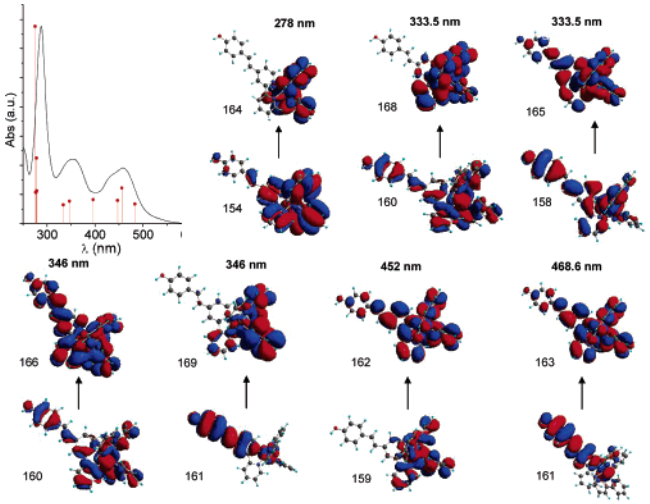

Figure 6. Experimental electronic spectra (black) and computed excitation energies and oscillator strengths (purple) at B3LYP/LANL2DZ in CH_3CN for receptor **1**. MOs involved in major transitions are shown.

Ru(II) polypyridyl complexes showed a good agreement with experiment.[29]

The TD-DFT excitation energies calculated for **1** as an acetonitrile solution are shown in Figure 6. The electronic spectrum for the receptor **1** showed transitions in the range 270−550 nm. Those around 280, 350, and 450 nm were particularly intense. The computed TD-DFT transition energies and their relative oscillator strengths matched the observed spectra quite well (Figure 6). The peak at ca. 280 nm was attributed mostly to intraligand $\pi_{bpy} \rightarrow \pi^*_{bpy}$ transitions, with minor contributions from $\pi_{L1} \rightarrow \pi^*_{bpy}$-based transitions. The signal at ca. 350 nm appears to have some MLCT $d\pi_{Ru} \rightarrow \pi^*_{L1}/\pi^*_{bpy}$ character, but the major contribution came from the ligand-based $\pi_{bpy} \rightarrow \pi^*_{bpy}/\pi_{L1} \rightarrow \pi^*_{bpy}$ excitations. The bands at 452 and 468 nm were also of mixed character, although the relative contribution from the $d\pi_{Ru} \rightarrow \pi^*_{bpy}/\pi^*_{L1}$-based MLCT transition was larger in this region. We believed the 350 nm transition to be due to an interligand-based process, but the TD-DFT calculations clearly indicate non-negligible contributions from MLCT transitions.

(29) (a) Fantacci, S.; Angelis, F. D.; Sgamellotti, A.; Re, N. *Chem. Phys. Lett*. **2004**, *396*, 43. (b) Fantacci, S.; Angelis, F. D.; Wang, J.; Bernhard, S.; Selloni, A. *J. Am. Chem. Soc*. **2004**, *126*, 9715. (c) Stoyanov, S. R.; Villegas, J. M.; Rillema, D. P. *Inorg. Chem*. **2002**, *41*, 2941. (d) Nazeeruddin, M. K.; Angelis, F. D.; Fantacci, S.; Selloni, A.; Viscardi, G.; Liska, P.; Ito, S.; Takeru, B.; Gratzel, M. *J. Am. Chem. Soc*. **2005**, *127*, 16835. (e) Lachaud, F.; Quaranta, A.; Pellegrin, Y.; Dorlet, P.; Charlot, M-C.; Un, S.; Leibl, W.; Auauloo, A. *Angew. Chem., Int. Ed*. **2005**, *44*, 1536.

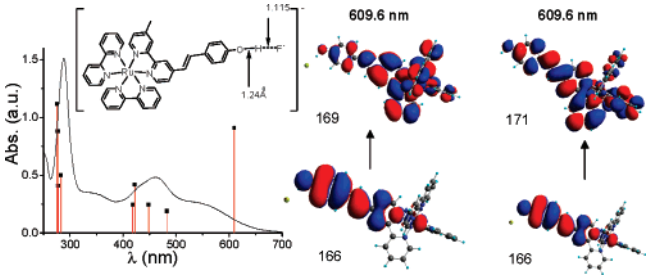

Figure 7. Experimental electronic spectra (black) and computed excitation energies and oscillator strengths (purple) at the B3LYP/LANL2DZ level for the optimized geometry of **1**···F^- in acetonitrile. Frontier molecular orbitals involved in electronic transitions for the 609 nm transition band are shown.

To examine the changes upon fluoride ion binding to receptor **1**, TD-DFT transition energies and relative oscillator strengths calculated at the optimized geometry of the complex are plotted in Figure 7. The optimized distances of 1.24 Å for O−H and 1.115 Å for H···F^- (Figure 7) indicate a strong ionic hydrogen bond.

The band around 280 nm which comes from intraligand $\pi_{bpy} \rightarrow \pi^*_{L1}$ and interligand $\pi_{L1} \rightarrow \pi^*_{bpy}$ transitions (Figure S11) was not affected much by fluoride binding (cf. Figures 6 and 7), while the other bands were red-shifted. According to the TD-DFT calculations for the complex, the bands in the intermediate range between 439 and 482 nm originated from $d\pi_{Ru} \rightarrow \pi^*_{bpy}$ MLCT, $\pi_{(bpy/L1)} \rightarrow \pi_{(bpy/\ L1)}$ intraligand, and $\pi_{(bpy/L1)} \rightarrow \pi^*_{(L1/bpy)}$ interligand excitations (Figure S11), while the lowest energy band at 609 nm was a mix of MLCT and inter/intraligand charge-transfer transitions: e.g. $\pi_{Ru} \rightarrow \pi^*_{(L1/bpy)}$ and $\pi_{(L1/bpy)} \rightarrow \pi^*_{(L1/bpy)}$ (Figure 7).

Experimentally, the lowest energy band for the complex $\mathbf{1}_{-H}^-$ appeared at 550 nm and was broad and intense compared to the 460 nm band in **1**. The TD-DFT calculations also showed a strong red-shift of the lowest energy transition upon F^- binding, from 468.6 nm (Figure 6) to 609.6 (Figure 7) nm, but they appeared to overestimate this effect given the comparison between the computed and observed transition wavelength (609 vs 550 nm). This would suggest that the calculations might overestimate the strength of the hydrogen bonding in the complex. To test this, we have modeled the interaction of F^- with a fixed receptor **1** by placing the F^- at a distance of 1.8 Å from the phenolic OH group. This distance corresponds to the energy minimum of the phenol/fluoride complex in a DFT optimization with fixed phenol geometry and the constraint of a linear hydrogen bond (Figure S12).

The TD-DFT transition energies and relative oscillator strengths for this model complex are shown in Figure 8 together with the observed spectrum. Compared to the free receptor **1** (Figure 6), the bands around 280 nm were again almost unaffected by fluoride binding in the model complex, while the other bands were again red-shifted but to a lesser extent than for the fully optimized complex (Figure 7). The calculated transitions in the range between 420 and 480 nm

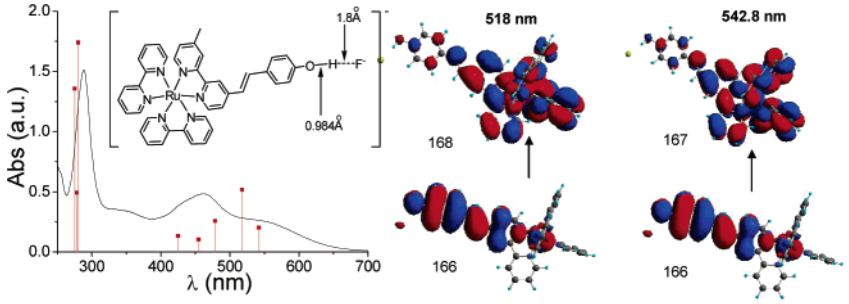

Figure 8. Experimental electronic spectra (black) and computed excitation energies and oscillator strengths (purple) at the B3LYP/LANL2DZ level for the model geometry of **1**.F^- in acetonitrile. Frontier molecular orbitals involved in electronic transitions for 518 and 542.8 nm are shown.

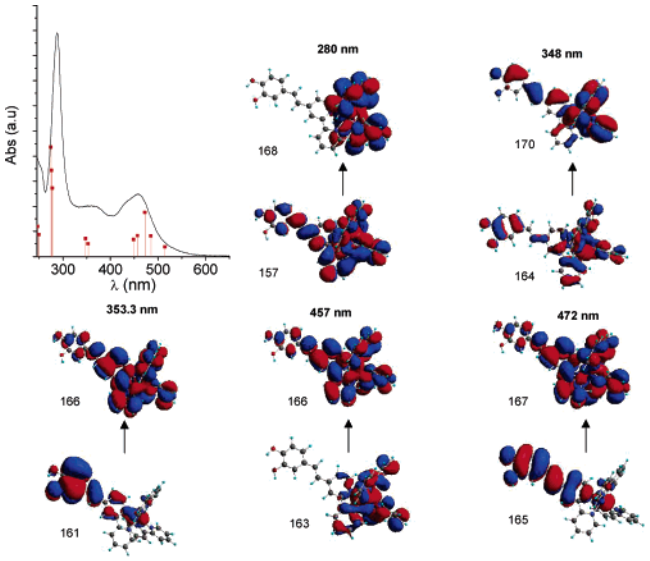

Figure 9. Experimental electronic spectra (black) and computed excitation energies and oscillator strengths (purple) at the B3LYP/LANL2DZ level in acetonitrile for receptor **2**. MOs involved in major transitions are shown.

matched quite well with experimental data (Figure 8), and the two lowest energy transitions computed at 518 and 542 nm were also close to the experimental value of 550 nm. These two transitions were of mixed character, combining $d\pi_{Ru} \rightarrow \pi^*_{(L1/bpy)}$ MLCT with interligand excitations [$\pi_{L1} \rightarrow \pi^*_{bpy}$], as in the case of the fully optimized complex. It is obvious from these calculations that the strength of the hydrogen-bonding interactions between the receptor and fluoride greatly affects the position of the lowest energy band(s) in the electronic spectrum. The better match between the computed spectral pattern for the model complex and the observed spectrum (Figure 8) suggested that structures with relatively weak $F^-\cdots H-O$ interactions were predominant in solution. In reality, there will be thermal motion, and many geometries will exist in solution, including those with compact geometeries as in the fully optimized complex (Figure 7). The latter will give rise to more red-shifted transitions and may, thus, be responsible for the low-energy tail in the observed spectrum.

The TD-DFT results for receptor **2** were analogous to those for receptor **1** and will therefore be only briefly addressed. The calculated electronic transitions for the free receptor **2** were again in good agreement with the observed spectrum (Figure 9).

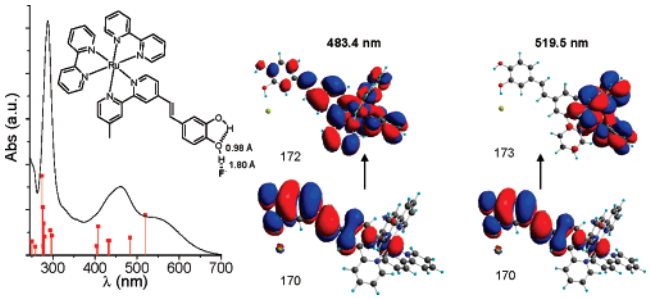

Figure 10. Experimental electronic spectra (black) and computed excitation energies and oscillator strengths (purple) at the B3LYP/LANL2DZ level for the model geometry of **2**$\cdots F^-$ in acetonitrile. Frontier molecular orbitals involved in electronic transitions for 483.4 and 519.5 nm are shown.

The 280 nm band is predominantly a result of intra- and interligand transitions, whereas the 340 and 450 nm bands originate from MLCT and intra- and inter ligand transitions (Figure 9). To explore the effects with fluoride binding, we considered again a fixed-geometry hydrogen-bonded model complex with F^- at a distance of 1.8 Å from the OH hydrogen atom of **2** (Figure 10). The calculated TD-DFT transitions are shown in Figure 10, together with the observed spectrum.

The low-energy bands show a significant red-shift, both experimentally and theoretically. The first band (experimental at 540 nm, TD-DFT at 519 nm) appeared to be a mixture of interligand charge-transfer and MLCT transitions, e.g., $\pi_{L2} \rightarrow \pi^*_{bpy}$ and $d\pi_{Ru} \rightarrow \pi^*_{bpy}$, similar to the situation discussed for receptor **1**.

Conclusions

This study demonstrated a rare example in which phenol and catechol functionalities can be used as an efficient colorimetric sensor for fluoride ions. Importantly, these complexes act as a colorimetric sensor even in presence of $\leq$20% H_2O (v/v). TD-DFT calculations in acetonitrile revealed that the origin of the newly developed spectral band upon complexation with F^- at 560 nm is due to the contributions from MLCT $d\pi_{Ru} \rightarrow \pi^*_{(L1/bpy)}$ and intra-/interligand transitions [$\pi_{L1} \rightarrow \pi^*_{bpy}$ and $\pi_{L1} \rightarrow \pi^*_{L1}$]. At higher concentrations of F^-, Brønsted acid−base interactions occurred, whereas, at relatively low concentration, hydrogen bonds between the O−H unit of the pendant phenol/catechol functionalities and F^- formed.

Acknowledgment. We thank the Department of Science and Technology (DST) and Board of Research in Nuclear

Science (BRNS) and the Government of India for supporting this work. D.A.J. acknowledges the CSIR for a Sr. Research Fellowship. A.D., B.G., and H.N.G. wish to thank Dr. P. K. Ghosh (CSMCRI, Bhavnagar, India) and Dr. T. Mukherjee (BARC, Mumbai, India) for their keen interest in this work. We thank the reviewers for their comments and suggestions that have helped us to improve the paper.

Supporting Information Available: Coordinates for optimized structures for receptors **1** (A) and **2** (B), changes in electronic spectra for receptors **1** (Figure S1) and **2** (Figure S2) in acetonitrile solution (at RT (room temperature)) on addition of different concentration ranges of [F^-], a spectrophotometric titration profile for receptors **1** (Figure S3) and **2** (Figure S4) with fluoride ions as titrant, changes in emission intensity for receptors **1** (Figure S5) and **2** (Figure S6) in acetonitrile solution (at RT) on addition of different concentration ranges of [F^-], changes in emission intensity for receptors **1** and **2** in acetonitrile solution (at RT) on addition of different concentration ranges of [OH^-] (Figure S7), change in ^{1}H NMR spectra of receptors **1** (Figure S8) and **2** (Figure S9) in CD_3CN (at RT) upon addition of F^-, changes in ^{19}F NMR spectra of receptors **1** (Figure S10) in CD_3CN (at RT) upon addition of F^-, changes in ^{1}H NMR spectra of L_1 and L_2 in DMSO-d_6 (at RT) with F^- (Figure S11), the general formula for calculating binding constants from UV−vis spectra, experimental electronic spectra and computed excitation energies and oscillator strengths at B3LYP/LANL2DZ in acetonitrile for the optimized structure of fluoride−receptor **1** complex where the orbitals involved in major transitions are shown (Figure S12), a plot for potential energy vs O−H···F^- distances for receptor **1** (Figure S13), and experimental electronic spectra and computed excitation energies and oscillator strengths at B3LYP/LANL2DZ in acetonitrile for the modeled structure of receptor **1** with O−H···F^- distances fixed at 1.8 Å where the orbitals involved in major transitions are shown (Figure S14). This material is available free of charge via the Internet at http://pubs.acs.org.

IC070165+